Biochem Biophys Res Commun. 2020 Nov 26; 533(1): 195–200. PMCID: PMC7486059
Published online 2020 Sep 11. doi: 10.1016/j.bbrc.2020.09.018 PMID: 32958250

Potent antiviral effect of silver nanoparticles on SARS-CoV-2

Sundararaj S. Jeremiah,[a] Kei Miyakawa,[a] Takeshi Morita,[a] Yutaro Yamaoka,[a,b] and Akihide Ryo[a,*]

Abstract

The pandemic of COVID-19 is spreading unchecked due to the lack of effective antiviral measures. Silver nanoparticles (AgNP) have been studied to possess antiviral properties and are presumed to inhibit SARS-CoV-2. Due to the need for an effective agent against SARS-CoV-2, we evaluated the antiviral effect of AgNPs. We evaluated a plethora of AgNPs of different sizes and concentration and observed that particles of diameter around 10 nm were effective in inhibiting extracellular SARS-CoV-2 at concentrations ranging between 1 and 10 ppm while cytotoxic effect was observed at concentrations of 20 ppm and above. Luciferase-based pseudovirus entry assay revealed that AgNPs potently inhibited viral entry step via disrupting viral integrity. These results indicate that AgNPs are highly potent microbicides against SARS-CoV-2 but should be used with caution due to their cytotoxic effects and their potential to derange environmental ecosystems when improperly disposed.

Keywords: Silver nanoparticles, Colloidal silver, SARS-CoV-2, COVID-19

1. Introduction

The elemental metal, Silver (Ag) has broad spectrum antimicrobial action against various bacteria, fungi and viruses. Due to their versatility, Ag nanoparticles (AgNP) have currently found their way as a microbicide for biological surfaces in various forms such as wound dressings, medical devices, deodorant sprays and fabrics. Several studies have demonstrated the potent antiviral action of AgNPs against various human pathogenic viruses such as Respiratory syncytial virus (RSV), Influenza virus, Norovirus, Hepatitis B virus (HBV) and Human immunodeficiency virus (HIV) [1]. In addition to these viruses, since Ag has been demonstrated to kill SARS-CoV, we hypothesized the strong possibility of AgNPs to inhibit SARS-CoV-2 [2,3]. Till date there are no studies directly demonstrating the effect of AgNPs on SARS-CoV-2. We tested colloidal silver (cAg), plain elemental Ag nanoparticles of different diameters ($AgNP_n$) and polyvinylpyrrolidone capped 10 nm silver nanoparticles ($PVP–AgNP_{10}$) against SARS-CoV-2 to find the most effective size and concentration of Ag that could inhibit SARS-CoV-2. We propose that AgNPs could be used on inanimate and non-biological surfaces to efficiently control the ongoing COVID-19 pandemic while simultaneously exercising care not to abuse it.

2. Materials and methods

2.1. Cell culture and virus propagation

VeroE6/TMPRSS2 (VeroE6 cells stably expressing the transmembrane serine protease TMPRSS2, JCRB #1819) and Calu-3 cell lines were cultured in DMEM containing 10% FBS [4]. SARS-CoV-2 (JPN/TY/WK-521) was obtained from NIID, JAPAN, stored in aliquots at −80 °C and handled in biosafety level 3 (BSL3). While performing SARS-CoV-2 infection studies, DMEM containing 2% FBS was used.

2.2. Plaque assay

Plaque assay was performed SARS-CoV-2 on VeroE6/TMPRSS2 and Calu-3 cell lines as described elsewhere with minor modifications [5]. 96-well plates were seeded with 5×10^4 cells per well in 10% FBS/DMEM and allowed to grow overnight. Viral solution was diluted in 10-fold serial dilutions in 2% FBS/DMEM. The supernatants from wells were removed and replaced with viral dilutions in correspondingly labeled wells and incubated at 37 °C for 96 h after which the cells were fixed with 4% formalin and stained with 0.25% crystal violet to visualize the plaques against a white background. Median tissue culture infecting dose (TCID50) and multiplicity of infection (MOI) were calculated from quadruplicate tests.

2.3. Silver formulations

PVP-$AgNP_{10}$ at 20 ppm stock concentration (Cat No: 795925) and cAg (Cat No: 85131) were obtained from Sigma. AgNPs of different sizes; $AgNP_2$ (Cat No: US7150), $AgNP_{15}$ (Cat No: US7091), $AgNP_{50}$, $AgNP_{80}$ and $AgNP_{100}$ (US1038W) were purchased from US Research Nanomaterials, Inc. All of the Silver formulations were dispersed in water and the desired concentration was prepared by diluting in sterile distilled water.

2.4. Cell viability assay

The CellTiter-Glo Cell Viability Assay (Promega) is a luminescence based assay which quantitatively detects live cells based on adenosine triphosphate (ATP) levels. Cell death subsequent to Ag mediated cytotoxicity or viral infection could be rapidly quantified using Cell-Titer Glo [6]. 50 µl of CellTiter-Glo Substrate (Promega) was added to the cells and their viability was measured based on the luminescence intensities detected by GloMax Discover System (Promega) 10 min later.

2.5. RT-qPCR

Viral RNA was extracted from culture supernatants using QIAamp viral RNA Mini Kit (Qiagen) and stored at −80 °C until further analysis. The extracted viral RNA was quantified using CFX96 Real-Time System (Bio-rad) with a TaqMan Fast virus 1-Step Master Mix (Thermo) using 5′-AAATTTTGGGGACCAGGAAC-3′ and 5′-TGGCAGCTGTGTAGGTCAA-3′ as the primer set and 5′-FAM-ATGTCGCGCATTGGCATGGA-BHQ-3′ as probe [7].

2.6. Cytotoxicity studies

cAg or AgNPs at desired concentration were added to VeroE6/TMPRSS2 or Calu-3 cell lines grown in 96-well white plates and were incubated at 37 °C for 48 or 96 h respectively after which the cells were washed with PBS and the viability was quantified using the CellTiter-Glo assay.

3. Silver and SARS-CoV-2 interaction studies

3.1. Virus pre-treatment assay

Virus at a MOI of 0.05 (for VeroE6/TMPRSS2) or 0.5 (for Calu-3) in DMEM containing 2% FBS was incubated with 2 ppm solution of AgNP for 1 h at 37 °C. The corresponding virus-AgNP mixture was added to VeroE6/TMPRSS2 or Calu-3 cells in 96 well plates and incubated for 48 h or 96 h respectively at 37 °C. Cell viability was quantified by CellTiter-Glo assay and the viral copies in supernatant were quantified by RT-qPCR.

3.2. Cell post-treatment assay

VeroE6/TMPRSS2 cells were infected with SARS-CoV-2 (MOI = 0.05) and incubated for 2 h at 37 °C. The wells were washed with PBS to remove extracellular viruses and topped up with DMEM containing 2% FBS with 2 ppm PVP-$AgNP_{10}$ and incubated for 48 h at 37 °C. Cell viability was quantified by CellTiter-Glo assay and the viral copies in supernatant were quantified by RT-qPCR.

3.3. Cell pre-treatment assay

VeroE6/TMPRSS2 cells were treated with 2 ppm PVP-AgNP$_{10}$ and incubated for 3 h at 37 °C. The wells were then washed with PBS to remove free AgNPs in medium and topped up with DMEM containing 2% FBS with SARS-CoV-2 (MOI = 0.05) and incubated for 48 h at 37 °C. Cell viability was quantified by CellTiter-Glo assay and the viral copies in supernatant were quantified by RT-qPCR.

3.4. Immunofluorescence

Cells were fixed with 4% paraformaldehyde and permeabilized with 0.5% Triton X-100, and then were blocked with Blocking One (Nacalai) at room temperature for 15 min. The cells were incubated with the polyclonal antibody against SARS-CoV-2 Nucleocapsid Protein antibody (1:100 dilution, Novus NB100-56576) at room temperature for 1 h. After incubation, cells were stained with Alexa 568-labeled anti-rabbit antibody (1:1000 dilution, Thermo) for 1 h at room temperature. The nucleus was stained with ProLong Gold Antifade Mountant with DAPI (Thermo). The images were taken by fluorescence microscope BZ-9000 (Keyence).

3.5. Pseudovirus entry assay

Pseudotype lentivirus was produced by transient transfection of HEK293 cells with pNL4-3. Luc.R-E− and pSARS2-Spike-FLAG at a ratio of 1:1. Culture supernatants containing pseudoviruses were collected 48 h after transfection and filtered through a 0.45 μm Millex-HV filter (Merck). For the entry assay, VeroE6/TMPRSS2 cells seeded in 96-well plates were washed and inoculated with 100 μl of medium containing pseudovirus with or without PVP-AgNP$_{10}$. Neutralizing antibody was used as a control for entry inhibition. 48 h after inoculation, cells were washed and added with 40 μl of Bright-Glo Substrate (Promega). Luciferase activity is measured with GloMax Discover System (Promega).

4. Results

4.1. Cytotoxicity, effective dose and contact time

AgNPs exhibit cytotoxicity to mammalian cells by generating reactive oxygen species (ROS) [8]. We wanted to assess the concentration dependent cytotoxicity exhibited by Ag on the cell lines VeroE6/TMPRSS2 (non-human origin) and Calu-3 (human lung epithelial cell). cAg was serially diluted and added to the cells in 96 well plates and the cell viability was assessed after 48 h using CellTiter-Glo assay. Ag was found to exhibit cytotoxicity at concentrations from 20 parts per million (ppm) onward in both VeroE6/TMPRSS2 (Fig. 1 A) and Calu-3 cell lines (Fig. 1B).

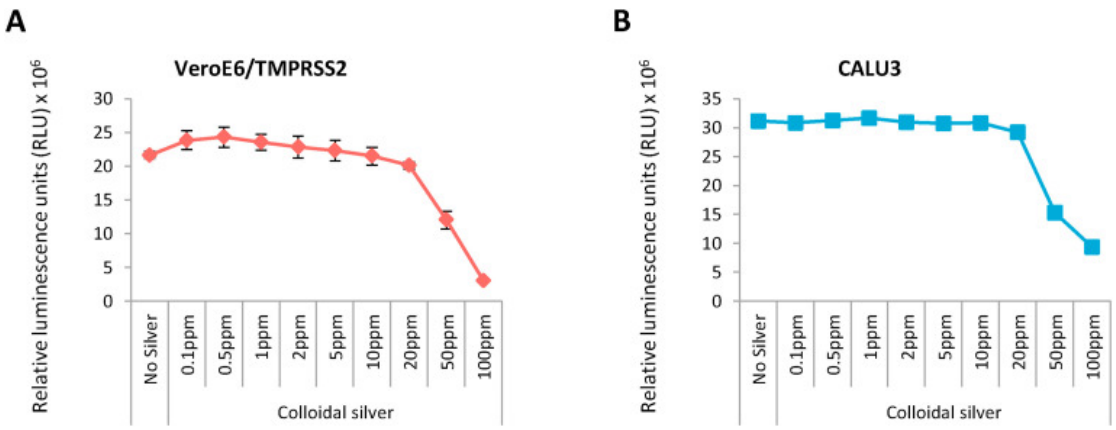

Open in a separate window

Fig. 1

Cytotoxicity of colloidal Silver on mammalian cells 1A: Cytotoxicity exhibited by serial concentrations of colloidal silver on VeroE6/TMPRSS2 cells. **1B**: Cytotoxicity exhibited by serial concentrations of colloidal silver on Calu-3 cells.

Since cAg contains particle sizes varying from 1 to 1000 nm, we used it as an initial screen to ascertain the effect of AgNPs on SARS-CoV-2. The multiplicity of infection (MOI) of SARS-CoV-2 was calculated by independent experiments and was found to be 0.05 and 0.5 for VeroE6/TMPRSS2 and Calu-3 respectively. Viral suspension at a fixed MOI was treated with each serial dilution of cAg for 1 h and then inoculated to VeroE6/TMPRSS2 and Calu-3 cells. Cell viability of infected VeroE6/TMPRSS2 was assessed after 48 h to identify the proportion of cells killed by the virus and the viral load was quantified in Calu-3 cells using real time reverse transcriptase quantitative polymerase chain reaction (RT-qPCR) after 96 h cAg showed robust antiviral effect denoted by increased viability of infected VeroE6/TMPRSS2 cells at concentrations ranging between 1 and 10 ppm (Fig. 2 A). In Calu-3 cells, significant viral load reduction was observed at similar cAg concentration range (Fig. 2B). While metal ions are known inhibitors of PCR at high concentrations, we confirmed that at the effective concentration (2 ppm), Ag did not inhibit amplification and is suitable to analyze viral RNA in Ag containing samples (Fig. S1) [9]. Since 2 ppm was also 10-fold lower than the cytotoxic concentration, it was chosen as the desired concentration for further testing.

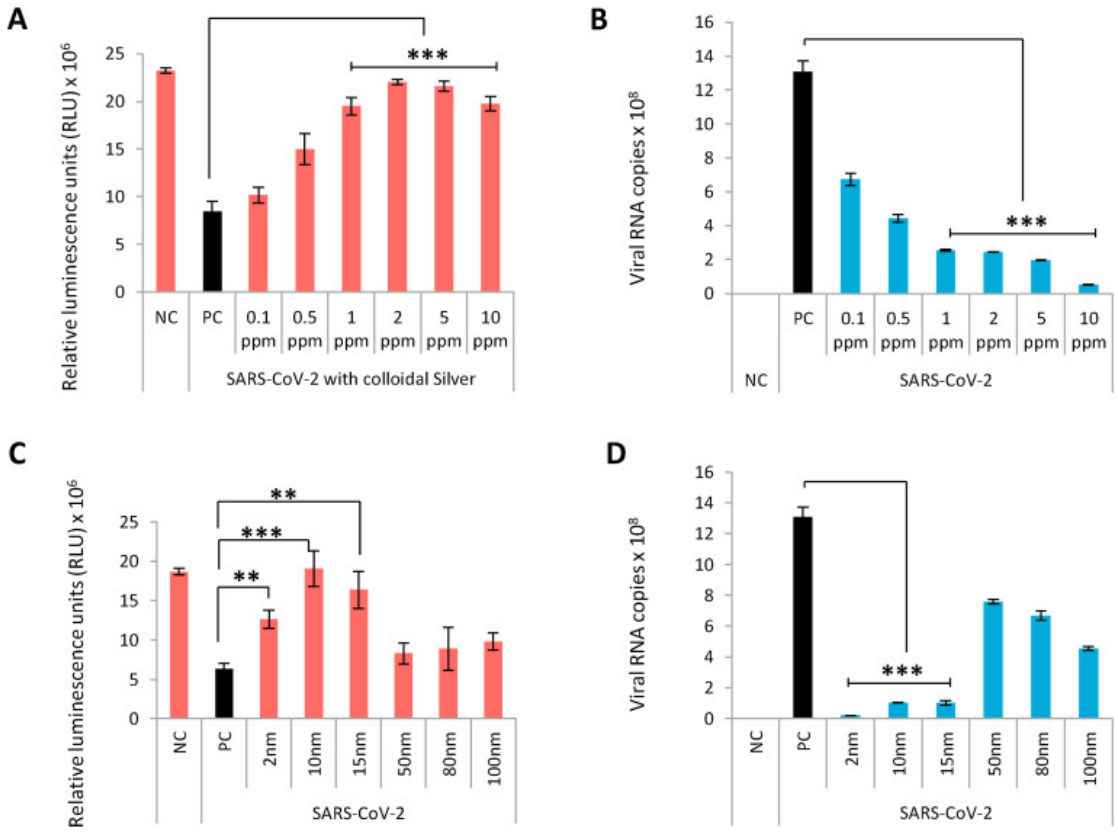

Open in a separate window

Fig. 2

Concentration and dose dependent antiviral effect of naked Silver nanoparticles on SARS-CoV-2.**2A:** Colloidal Silver rescues VeroE6/TMPRSS2 cells from SARS-CoV-2 mediated cell death in a concentration dependent manner. Error bars obtained from triplicate testing. p value ≤ 0.005 (∗∗∗). **2B:** Concentration dependent inhibition of SARS-CoV-2 replication in Calu-3 cells by colloidal Silver. Error bars obtained from triplicate testing. *p* value ≤ 0.001 (∗∗∗). **2C**: Silver nanoparticles exhibit size-dependent antiviral action against SARS-CoV-2 in Vero/TMPRSS2 cells. Error bars obtained from triplicate testing. *p* value ≤ 0.005 (∗∗∗). **2D**: Size-dependent viral inhibition of SARS-CoV-2 by Silver nanoparticles in Calu-3 cells. Error bars obtained from triplicate testing. *p* value ≤ 0.001 (∗∗∗).

Previous studies have documented the size dependent potency of AgNPs in viral inactivation, with ≤10 nm particle size reported to have maximum antiviral effect [10]. Since cAg contains varying sizes of Ag particles, we predicted that the particles around 10 nm size in cAg would have exerted the antiviral effect. To prove this, we employed the virus pre-treatment assay (VPrA) to test antiviral effect of AgNPs of different sizes ranging from 2 to 100 nm on extracellular viruses. Virus was treated with 2 ppm solution of AgNPs of different sizes for 1 h and the virus-AgNP mixture was added to VeroE6/TMPRSS2 and Calu-3 cells. The cell viability was quantified by CellTiter-Glo assay in VeroE6/TMPRSS2 and the viral copies in supernatant were quantified by RT-qPCR in Calu-3 cells. Antiviral effect was noted with AgNPs of size ranging from 2 to 15 nm (Fig. 2C and D). $AgNP_2$ showed cytotoxicity at 2 ppm while other sizes did not (Fig. S2). Hence we chose PVP-$AgNP_{10}$ for further testing. Since we observed excellent antiviral activity in VPrA at 1 h, we wanted to know the minimum contact time required by Ag for viral inhibition. Time course study performed based on VPrA with PVP-$AgNP_{10}$ revealed significant inhibition beyond 30 min of contact (Fig. S3).

4.2. Silver inhibits extracellular viruses by preventing viral entry

We next performed the VPrA, cell post-treatment assay (CPoA) and the cell pre-treatment assay (CPrA) on SARS-CoV-2 using PVP-AgNP$_{10}$ in VeroE6/TMPRSS2 to observe the effect of Ag on extracellular and intracellular viruses (Fig. 3 A). VPrA showed effective inhibition of extracellular free virions characterized by both the reduction of cell death and also a steep fall in the viral load to negligible levels (Fig. 3B and C). We further performed the CPoA to detect the ability of Ag to suppress virus in already infected cells. In this experimental design, VeroE6/TMPRSS2 cells were allowed to be infected with SARS-CoV-2 (MOI 0.05) for2 hours after which the extracellular viruses were washed and then the infected cells were treated with 2 ppm of PVP-AgNP$_{10}$. We observed significant protection of infected cells and suppression of viral load with PVP-AgNP$_{10}$ (Fig. 3B and C). Additionally we performed the CPrA to assess the ability of silver pre-treated cells to resist viral infection. VeroE6/TMPRSS2 cells were incubated with 2 ppm PVP-AgNP$_{10}$ for 3 h after which the cells were washed to remove unbound silver followed by infection with SARS-CoV-2 (MOI 0.05). At the end of 48 h, the virus was found only to be partially inhibited (Fig. 3C).

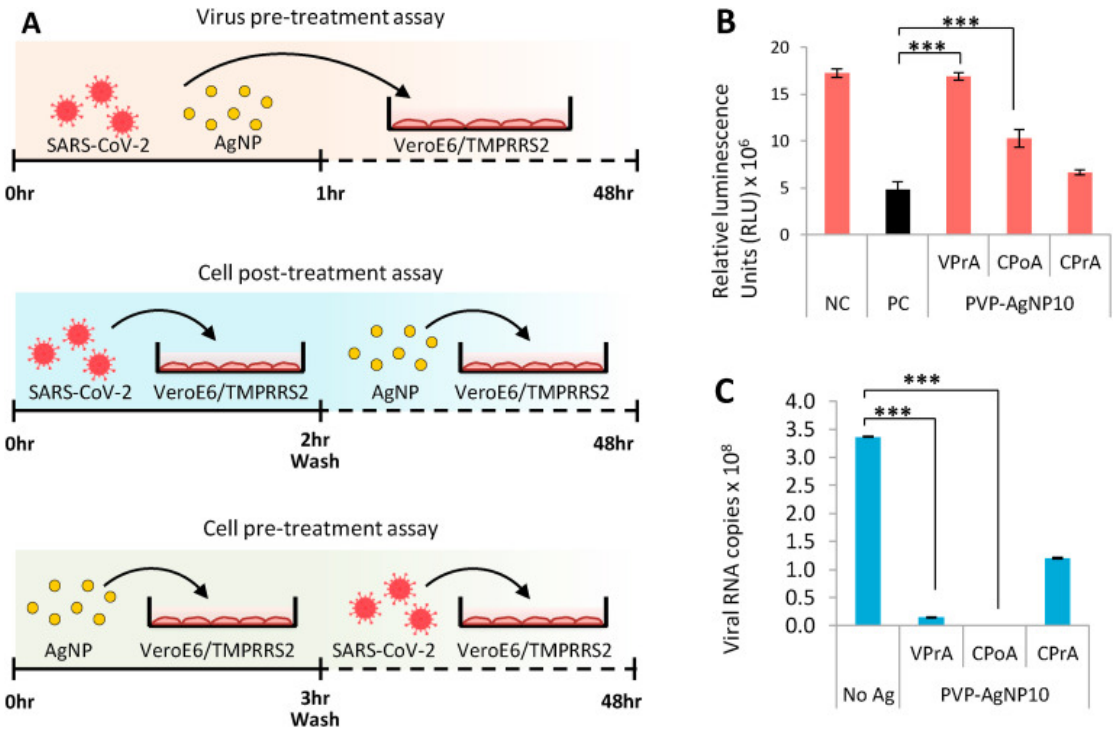

Open in a separate window

Fig. 3

Silver nanoparticles effectively inhibit extracellular SARS-CoV-2.**3A**: Schematic representation of virus pre-treatment assay (top panel), cell post-treatment assay (central panel) and cell pre-treatment assay (bottom panel). **3B**: Performance of PVP coated 10 nm Silver nanoparticles in the three study designs with respect to rescue of cells from SARS-CoV-2 infection. Error bars obtained from triplicate testing. *p* value ≤ 0.005 (***). **2C**: Performance of PVP coated 10 nm Silver nanoparticles in the three study designs with respect to reduction of SARS-CoV-2 replication. Error bars obtained from triplicate testing. *p* value ≤ 0.001 (***).

We confirmed the size dependent antiviral effect of PVP- AgNP$_{10}$ using the immunofluorescence analysis carried on VPrA experimental model; SARS-CoV-2 infection was effectively averted by AgNP$_{10}$ and not by AgNP$_{100}$ (Fig. 4 A). The plaque assay revealed that silver achieved complete inhibition of 0.05 MOI which is one log$_{10}$ fold more than virus control. Partial inhibition was observed with higher viral loads starting from 0.5 MOI (Fig. 4B). To assess the role of AgNPs in viral entry, we

performed the luciferase based pseudovirus entry assay. PVP-AgNP$_{10}$ potently inhibited pseudoviral entry characterized by significant reduction of luciferase activity similar to that of the neutralizing antibody used as control (Fig. 4C).

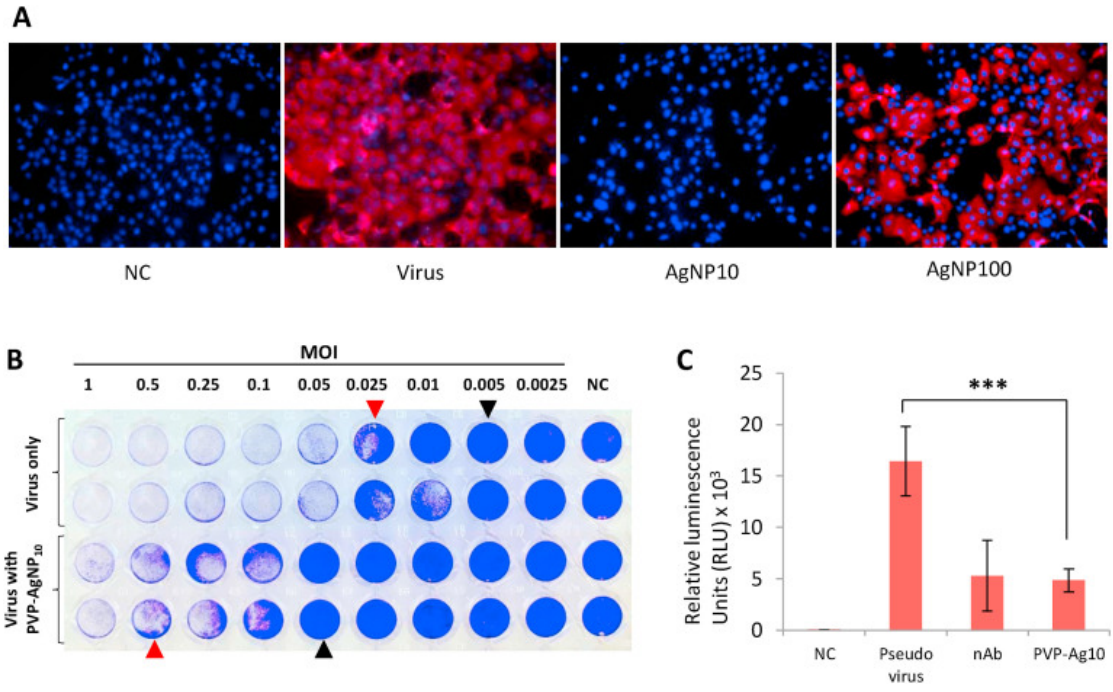

Open in a separate window

Fig. 4

Characteristics of PVP coated 10 nm Silver nanoparticles in SARS-CoV-2 infection. **4A**: Immunofluorescence imaging comparing the effect of 10 nm and 100 nm Silver nanoparticles against SARS-CoV-2 infection in VeroE6/TMPRSS2 cells. Cell nuclei (blue) and SARS-CoV-2 nucleocapsid protein in cytoplasm (red). NC - Negative control. **4B**: PVP coated 10 nm Silver nanoparticles protect VeroE6/TMPRSS2 cells from SARS-CoV-2 infection mediated cell death. Crystal violet staining reveals partial protection with visible plaques (red arrowheads) and complete protection with absence of plaques (black arrowheads). **4C**: Pseudovirus entry assay. PVP coated 10 nm Silver nanoparticles inhibit entry of pseudovirus in VeroE6/TMPRSS2 cells. NC - Negative control, nAb - Neutralizing antibody. (For interpretation of the references to colour in this figure legend, the reader is referred to the Web version of this article.)

5. Discussion

Ag is long known for its antimicrobial effect and the antiviral property of AgNPs is being extensively researched with renewed interest in the recent past [1]. The exact mechanism by which AgNPs exert its killing effect on viruses is still obscure. However, it has been consistently observed that AgNPs interact with the structural proteins on the surface of extracellular viruses to inhibit infection in the early phase, by either preventing viral attachment or entry, or by damaging the surface proteins to affect the structural integrity of virions [11,12]. In the current study, we have obtained similar findings in the VPrA where AgNPs effectively inhibits extracellular SARS-CoV-2 to protect the target cells from infection and the pseudovirus entry assay revealed that AgNPs interfere with viral entry.

AgNPs have been shown to preferentially bind to viral surface proteins rich in sulfhydryl groups and cleave the disulfide bonds to destabilize the protein, thereby affecting viral infectivity [11,13]. Studies on HIV have shown that AgNPs associate to the disulfide bonds that are in close proximity to the CD4

binding domain of the gp120 surface protein [11]. Hati and Bhattacharyya have demonstrated the importance disulfide bonds in binding of SARS-CoV-2 spike protein with the angiotensin converting enzyme-2 (ACE2) receptor and the disruption of which lead to impaired viral binding to the receptor [14]. Considering the mechanism of action of AgNPs shown by other authors, it can be presumed that AgNPs exert their antiviral effect on SARS-CoV-2 by disrupting the disulfide bonds on the spike protein and ACE2 receptors. Further studies are being conducted to find the antiviral mechanism of AgNPs on SARS-CoV-2 and elucidate it in detail subsequently.

AgNPs have also been claimed to possess intracellular antiviral action by interacting with viral nucleic acids [15]. We observed a partial antiviral effect in CPrA, as there was some amount of reduction in the viral load in cells pre-treated with PVP-$AgNP_{10}$. While the reason for this effect is not known at present, it is possibly explained to be either due to the destruction of disulfide bridges on ACE2 receptor or due to a true intracellular mechanism (there by inhibiting serial viral infection of newly produced virus from infected cells to uninfected cells). Also, since Ag binds non-specifically to proteins, their use as antiviral agents might also cause some cellular dysfunction. Further studies are required to more precisely explain the holistic effect of Ag *in vivo*.

Several studies have reiterated the size dependent antiviral effect of AgNPs with particles around 10 nm diameter being most effective [1]. This has been attributed the higher stability of interaction to the viral protein achieved by 10 nm particles which is not capable by larger particles [11]. Consistent with this, we also observed *anti*-SARS-CoV-2 activity only with AgNPs of diameters ranging from 2 to 15 nm. Our immunofluorescence study corroborated the above phenomenon, as we observed that PVP-$AgNP_{10}$ completely inhibited SARS-CoV-2 but $AgNP_{100}$ did not.

AgNPs can be generated by several methods and can contain reducing agents and capping agents along with the metal particles [16]. Coated or capped AgNPs are found to be more advantageous than plain AgNPs as coating increases stability, decreases agglomeration and reduces cytotoxicity of AgNPs [17]. Among the coated AgNPs, PVP capped nanoparticles are widely studied for biological use. It has been observed that PVP coating of AgNPs does not hinder their antiviral activity while other coating agents do [18]. PVP-$AgNP_{10}$ has been demonstrated to possess excellent antiviral activity against enveloped viruses such as RSV and HIV [11,19]. This was the rationale to select PVP-$AgNP_{10}$ for the study and we have demonstrated the robust antiviral effect of PVP-$AgNP_{10}$ against SARS-CoV-2.

Antiviral effect of AgNPs is also concentration dependent. Most studies have observed the antiviral efficacy of AgNPs at concentrations ranging between 10 and 100 ppm [1]. However, 0.5 ppm cAg has been shown effective in inhibiting Influenza virus and is the least concentration that has been reported to show antiviral activity [20]. In the current study, we observed naked AgNPs to inhibit SARS-CoV-2 at concentrations ranging between 1 and 10 ppm and become cytotoxic to mammalian cells from 20 ppm and above.

Cytotoxicity of AgNPs to mammalian cells depends on the cell type and also the type of AgNPs. Mehrbod et al. have observed cytotoxicity in Madin-Darby Canine Kidney (MDCK) cells with naked cAg particles at concentrations higher than 0.5 ppm [20]. Naked AgNPs with NaBH4 reducing agent were found to induce apoptosis in colon adenocarcinoma cells at 11 ppm, while Citrate-stabilized naked AgNPs have been observed to exhibit cytotoxicity at concentrations higher than 30 ppm [21,22]. In this regard, PVP coated AgNPs have been demonstrated to be the least cytotoxic with no demonstrable cytotoxicity even at 50 ppm in human alveolar basal epithelial cells [19]. Smaller particles have a higher toxic potential due to the greater surface area of interaction with the bound protein [23]. We observed this effect as $AgNP_2$ showed cytotoxicity even at 2 ppm while none of the bigger particles were cytotoxic at this concentration. Therefore, care should be exercised when Ag is used on biological surfaces.

Various ingestible and inhalable formulations of Ag are being marketed as cure for COVID-19, which available to purchase over the counter. The cytotoxic potential of these formulations should be considered before personal use. Also, Ag is a very broad spectrum microbicide. Illicit use of Ag might

create an imbalance in the commensal microbiota leading to unforeseen consequences [24]. AgNPs can be used on a variety of inanimate surfaces to combat the ongoing COVID-19 pandemic [3]. Ag coated masks have been found to be effective in inhibiting SARS-CoV-2 and could potentially be effective when applied on the air filters of air conditioners and medical devices [25]. AgNP incorporated polycotton fabrics have been proven to inhibit SARS-CoV-2 [26]. Ag based sanitizers and disinfectants are also being used for disinfection of hands and inanimate surfaces respectively [27]. However, the effect of AgNPs on influencing the microbial life when released in the environment is unknown [16]. A proper disposal protocol should be developed for Ag containing products to avoid causing untoward imbalances in the environmental microbial pattern when discarded after use.

Declaration of competing interest

The authors have no conflicts of interest directly relevant to the content of this article. Y.Y. is a current employee of Kanto Chemical Co., Inc.

Acknowledgements

The study was funded by Japan Agency for Medical Research and Development (AMED), Grant number: 19fk0108110h0401 and 20he0522001j0001.

Footnotes

Appendix A Supplementary data to this article can be found online at https://doi.org/10.1016/j.bbrc.2020.09.018.

Appendix A. Supplementary data

The following is the Supplementary data to this article:

Multimedia component 1:

Click here to view.(73K, docx) Multimedia component 1

References

1. Galdiero S., Falanga A., Vitiello M., Cantisani M., Marra V., Galdiero M. Silver nanoparticles as potential antiviral agents. *Mol. Basel Switz.* 2011;16:8894–8918. [PMC free article] [PubMed] [Google Scholar]

2. Han J., Chen L., Duan S.-M., Yang Q.-X., Yang M., Gao C., Zhang B.-Y., He H., Dong X.-P. Efficient and quick inactivation of SARS coronavirus and other microbes exposed to the surfaces of some metal catalysts. *Biomed. Environ. Sci. BES.* 2005;18:176–180. [PubMed] [Google Scholar]

3. Talebian S., Wallace G.G., Schroeder A., Stellacci F., Conde J. Nanotechnology-based disinfectants and sensors for SARS-CoV-2. *Nat. Nanotechnol.* 2020;15:618–621. [PubMed] [Google Scholar]

4. Matsuyama S., Nao N., Shirato K., Kawase M., Saito S., Takayama I., Nagata N., Sekizuka T., Katoh H., Kato F., Sakata M., Tahara M., Kutsuna S., Ohmagari N., Kuroda M., Suzuki T., Kageyama T., Takeda M. Enhanced isolation of SARS-CoV-2 by TMPRSS2-expressing cells. *Proc. Natl. Acad. Sci. U.S.A.* 2020;117:7001–7003. [PMC free article] [PubMed] [Google Scholar]

5. Gordon D.E., Jang G.M., Bouhaddou M., Xu J., Obernier K., White K.M., O'Meara M.J., Rezelj V.V., Guo J.Z., Swaney D.L., Tummino T.A., Hüttenhain R., Kaake R.M., Richards A.L., Tutuncuoglu B., Foussard H., Batra J., Haas K., Modak M., Kim M., Haas P., Polacco B.J., Braberg H., Fabius J.M., Eckhardt M., Soucheray M., Bennett M.J., Cakir M., McGregor M.J., Li Q., Meyer B., Roesch F., Vallet T., Mac Kain A., Miorin L., Moreno E., Naing Z.Z.C., Zhou Y., Peng S., Shi Y., Zhang Z., Shen W., Kirby I.T., Melnyk J.E., Chorba J.S., Lou K., Dai S.A., Barrio-Hernandez I., Memon D., Hernandez-Armenta C., Lyu J., Mathy C.J.P., Perica T., Pilla K.B., Ganesan S.J., Saltzberg D.J., Rakesh R., Liu X., Rosenthal S.B., Calviello L., Venkataramanan S., Liboy-Lugo J., Lin Y., Huang X.-

P., Liu Y., Wankowicz S.A., Bohn M., Safari M., Ugur F.S., Koh C., Savar N.S., Tran Q.D., Shengjuler D., Fletcher S.J., O'Neal M.C., Cai Y., Chang J.C.J., Broadhurst D.J., Klippsten S., Sharp P.P., Wenzell N.A., Kuzuoglu-Ozturk D., Wang H.-Y., Trenker R., Young J.M., Cavero D.A., Hiatt J., Roth T.L., Rathore U., Subramanian A., Noack J., Hubert M., Stroud R.M., Frankel A.D., Rosenberg O.S., Verba K.A., Agard D.A., Ott M., Emerman M., Jura N., von Zastrow M., Verdin E., Ashworth A., Schwartz O., d'Enfert C., Mukherjee S., Jacobson M., Malik H.S., Fujimori D.G., Ideker T., Craik C.S., Floor S.N., Fraser J.S., Gross J.D., Sali A., Roth B.L., Ruggero D., Taunton J., Kortemme T., Beltrao P., Vignuzzi M., García-Sastre A., Shokat K.M., Shoichet B.K., Krogan N.J. A SARS-CoV-2 protein interaction map reveals targets for drug repurposing. *Nature.* 2020;583:459–468. [PMC free article] [PubMed] [Google Scholar]

6. Noah J.W., Severson W., Noah D.L., Rasmussen L., White E.L., Jonsson C.B. A cell-based luminescence assay is effective for high-throughput screening of potential influenza antivirals. *Antivir. Res.* 2007;73:50–59. [PubMed] [Google Scholar]

7. Shirato K., Nao N., Katano H., Takayama I., Saito S., Kato F., Katoh H., Sakata M., Nakatsu Y., Mori Y., Kageyama T., Matsuyama S., Takeda M. Development of genetic diagnostic methods for detection for novel coronavirus 2019(nCoV-2019) in Japan. *Jpn. J. Infect. Dis.* 2020;73:304–307. [PubMed] [Google Scholar]

8. Lanone S., Boczkowski J. Biomedical applications and potential health risks of nanomaterials: molecular mechanisms. *Curr. Mol. Med.* 2006;6:651–663. [PubMed] [Google Scholar]

9. Combs L.G., Warren J.E., Huynh V., Castaneda J., Golden T.D., Roby R.K. The effects of metal ion PCR inhibitors on results obtained with the Quantifiler(®) Human DNA Quantification Kit. *Forensic Sci. Int. Genet.* 2015;19:180–189. [PubMed] [Google Scholar]

10. Lara H.H., Ayala-Nuñez N.V., Ixtepan-Turrent L., Rodriguez-Padilla C. Mode of antiviral action of silver nanoparticles against HIV-1. *J. Nanobiotechnol.* 2010;8:1. [PMC free article] [PubMed] [Google Scholar]

11. Elechiguerra J.L., Burt J.L., Morones J.R., Camacho-Bragado A., Gao X., Lara H.H., Yacaman M.J. Interaction of silver nanoparticles with HIV-1. *J. Nanobiotechnol.* 2005;3:6. [Google Scholar]

12. Swathy J.R., Sankar M.U., Chaudhary A., Aigal S., Anshup null, Pradeep T. Antimicrobial silver: an unprecedented anion effect. *Sci. Rep.* 2014;4:7161. [PMC free article] [PubMed] [Google Scholar]

13. Kim J., Yeom M., Lee T., Kim H.-O., Na W., Kang A., Lim J.-W., Park G., Park C., Song D., Haam S. Porous gold nanoparticles for attenuating infectivity of influenza A virus. *J. Nanobiotechnol.* 2020;18 54. [PMC free article] [PubMed] [Google Scholar]

14. Hati S., Bhattacharyya S. Impact of thiol-disulfide balance on the binding of Covid-19 spike protein with angiotensin-converting enzyme 2 receptor. *ACS Omega.* 2020;5:16292–16298. [PMC free article] [PubMed] [Google Scholar]

15. Lu L., Sun R.W.-Y., Chen R., Hui C.-K., Ho C.-M., Luk J.M., Lau G.K.K., Che C.-M. Silver nanoparticles inhibit hepatitis B virus replication. *Antivir. Ther.* 2008;13:253–262. [PubMed] [Google Scholar]

16. Wei L., Lu J., Xu H., Patel A., Chen Z.-S., Chen G. Silver nanoparticles: synthesis, properties, and therapeutic applications, Drug Discov. *Today Off.* 2015;20:595–601. [PMC free article] [PubMed] [Google Scholar]

17. Fahmy H.M., Mosleh A.M., Elghany A.A., Shams-Eldin E., Serea E.S.A., Ali S.A., Shalan A.E. Coated silver nanoparticles: synthesis, cytotoxicity, and optical properties. *RSC Adv.* 2019;9 [Google Scholar]

18. Zheng Y., Cloutier P., Hunting D.J., Sanche L. Radiosensitization by gold nanoparticles: comparison of DNA damage induced by low and high-energy electrons. *J. Biomed. Nanotechnol.* 2008;4:469–475. [Google Scholar]

19. Morris D., Ansar M., Speshock J., Ivanciuc T., Qu Y., Casola A., Garofalo R. Antiviral and immunomodulatory activity of silver nanoparticles in experimental RSV infection. *Viruses.* 2019;11 [PMC free article] [PubMed] [Google Scholar]

20. Mehrbod P., Motamed N., Tabatabaian M., Estyar R.S., Amini E., Shahidi M., Kheiri M.T. In vitro antiviral effect of "nanosilver" on influenza virus. *DARU J. Pharm. Sci.* 2015;17:88–93. [Google Scholar]

21. Gopinath P., Gogoi S.K., Chattopadhyay A., Ghosh S.S. Implications of silver nanoparticle induced cell apoptosis for in vitro gene therapy. *Nanotechnology.* 2008;19 [PubMed] [Google Scholar]

22. Bekele A.Z., Gokulan K., Williams K.M., Khare S. Dose and size-dependent antiviral effects of silver nanoparticles on feline Calicivirus, a human Norovirus surrogate. *Foodb. Pathog. Dis.* 2016;13:239–244. [PubMed] [Google Scholar]

23. Johnston H.J., Hutchison G., Christensen F.M., Peters S., Hankin S., Stone V. A review of the in vivo and in vitro toxicity of silver and gold particulates: particle attributes and biological mechanisms responsible for the observed toxicity. *Crit. Rev. Toxicol.* 2010;40:328–346. [PubMed] [Google Scholar]

24. Williams K., Milner J., Boudreau M.D., Gokulan K., Cerniglia C.E., Khare S. Effects of subchronic exposure of silver nanoparticles on intestinal microbiota and gut-associated immune responses in the ileum of Sprague-Dawley rats. *Nanotoxicology.* 2015;9:279–289. [PubMed] [Google Scholar]

25. Balagna C., Perero S., Percivalle E., Nepita E.V., Ferraris M. Virucidal effect against coronavirus SARS-CoV-2 of a silver nanocluster/silica composite sputtered coating. *Open Ceram.* 2020;1:100006. [Google Scholar]

26. Tremiliosi G.C., Simoes L.G.P., Minozzi D.T., Santos R.I., Vilela D.C.B., Durigon E.L., Machado R.R.G., Medina D.S., Ribeiro L.K., Rosa I.L.V., Assis M., Andrés J., Longo E., Freitas-Junior L.H. Ag nanoparticles-based antimicrobial polycotton fabrics to prevent the transmission and spread of SARS-CoV-2. *BioRxiv.* 2020:2020. 06.26.152520. [Google Scholar]

27. Vazquez-Munoz R., Lopez-Ribot J.L. Nanotechnology as an alternative to reduce the spread of COVID-19. *Challenges.* 2020;11:15. [Google Scholar]